Full-field multidimensional deconvolution to retrieve body-wave reflections from sparse passive sources

Hartstra, Iris; Almagro Vidal, Carlos; Wapenaar, Kees

Important note
To cite this publication, please use the final published version (if applicable).
Please check the document version above.

Full-field multidimensional deconvolution to retrieve body-wave reflections from sparse passive sources

I.E. Hartstra, C. Almagro Vidal and K. Wapenaar

Department of Geoscience and Engineering, Delft University of Technology, P.O. Box 5048, 2600 GA Delft, The Netherlands. E-mail: i.e.hartstra@tudelft.nl

SUMMARY

Our objective is to complement lithospheric seismic tomography with an interferometric method to retrieve high-resolution reflectivity images from local earthquake recordings. The disadvantage of using local earthquakes for the retrieval of reflected body-waves is their usual sparse distribution. We propose an alternative formulation of passive seismic interferometry by multidimensional deconvolution (MDD) which uses the multiples in the full recordings to compensate for missing illumination angles. This method only requires particle-velocity recordings at the surface from passive transient sources and retrieves body-wave reflection responses without free-surface multiples. We conduct an acoustic modelling experiment to compare this formulation to a previous MDD method and Green's function retrieval by cross-correlation for different source distributions. We find that in the case of noise-contaminated recordings obtained under severely limited and irregular illumination conditions, the alternative MDD method introduced here still retrieves the complete reflection response without free-surface multiples where the other interferometric methods break down.

Key words: Interferometry; Body waves; Coda waves.

1 INTRODUCTION

Seismic tomography is used extensively to obtain information about the complex low-frequency structures of the lithosphere (Nolet 2008). Reflection imaging could complement tomography by providing a well-constrained image of impedance contrasts with a high spatial resolution. A densely sampled reflection survey with controlled high-frequency sources placed at the surface could yield this desired image. However, conducting this type of survey at a lithospheric scale is very expensive and invasive for the natural environment.

Seismic interferometry (SI) represents a set of less expensive and non-invasive methods that can be applied to a regular and densely sampled receiver array at the surface to retrieve virtual body-wave reflection responses from passive recordings (Schuster 2009). These methods have the potential to give accurate results when specific requirements are met. For example, they rely on sufficient and isotropic illumination by naturally occurring seismic sources. Local earthquakes have the potential to provide waves with high-frequency content. However, the range of illumination angles provided by these sources strongly depends on their relative position and orientation to the imaging target and the receiver array. Multiple reflections could compensate for the missing illumination angles, but the currently employed SI methods are not designed to utilize higher order scattering events in a physically correct way to construct body-wave reflections.

SI by crosscorrelation retrieves any type of Green's function response between two receivers, by effectively turning one of the receivers into a virtual source. In practice, this method has proven to yield body-wave reflections under specific circumstances (Draganov *et al.* 2007; Tonegawa *et al.* 2009; Poli *et al.* 2012; Boué *et al.* 2014). However, there are several drawbacks to consider when using crosscorrelation for the retrieval of body waves. First of all, the method requires a well-sampled boundary of passive sources to enclose the receiver array. In addition, the source mechanisms and radiation patterns should ideally be the same for all passive sources. Violation of these requirements leads to irregular illumination of the array, which in turn causes the radiation patterns of the virtual-sources to be anisotropic. This inevitably leaves its imprint on the retrieved reflection responses by causing inaccurate reconstruction of amplitudes as well as a less effective destructive interference of artefacts. Finally, SI by crosscorrelation assumes the input wavefields to be reversible in time, which only holds in lossless media. This implies that for the case of field data the reliability of this method is compromised since it is unlikely that all these conditions are met.

Multidimensional deconvolution (MDD) offers an alternative to crosscorrelation for retrieving reflection responses from passive recordings (Wapenaar *et al.* 2008). This method does not rely on time-reversibility, because it is based on reciprocity relations of the convolution type. Intuitively, MDD can be compared to a 'deblurring' procedure whereby artefacts caused by anisotropic illumination or variations in passive-source mechanisms are corrected for by deconvolving with a 'point-spread function' (PSF). This PSF is constructed from the wavefields of the kernel in the original reciprocity formulation and ideally contains spectral information of the virtual-source radiation patterns (van der Neut 2012). The kernel

of the reciprocity formulation of the MDD method described in Wapenaar *et al.* (2008) is, in theory, composed of the direct wave and the internal multiples from the recorded wavefield. However, when the subsurface reflectivity is unknown, it is in practice only feasible to extract the direct wave (which can include possible short-period multiples) from the recordings, because separating internal multiples from surface-related multiples is not a trivial task. The resulting approximation of the kernel limits the PSF to wavenumbers provided by the directly incident field: the 'ballistic field' (Nakata *et al.* 2014). Inverting this ballistic PSF likely produces errors, because the function is inexact and affected by time-window procedures. These disadvantages are expected to be most apparent when the passive-source illumination from approximately vertically below the receiver array is absent and the retrieval of virtual reflections relies on low-wavenumber illumination from scattered events in the passive coda wavefield. In such a case, a purely ballistic PSF does not suffice to compensate for irregularities in the virtual-source radiation patterns. In fact, the PSF would require spectral information of the coda wavefield as well in order to enable the appropriate illumination balancing and thus enhance the sought-after virtual reflection responses.

The need for a more extensive PSF led to the development of an alternative reciprocity relation which contains an exact full-field kernel, instead of an approximated ballistic one (Almagro Vidal 2017). Here, the term 'full-field' indicates that the kernel consists of the entire recorded passive wavefield containing both the ballistic and coda field. The full-field MDD method thus conducts the 'deblurring' operation using a full-field PSF, which has encoded the maximum available spectral information to correct the virtual-source radiation patterns. Consequently, in cases when the retrieval of virtual reflections relies primarily on illumination from the passive coda field, this full-field PSF is expected to perform better than the ballistic PSF. Moreover, the full-field PSF avoids inversion of an approximated and time-windowed function (as is the case in ballistic MDD).

In order to validate the above-mentioned advantages of full-field MDD over ballistic MDD and crosscorrelation, we conduct an effective comparison of these SI methods. The experiments are carried out using acoustic synthetic data, which allows for a controlled analysis of the performance of each of these methods under various passive-source illumination conditions as well as noise contamination.

2 METHODS

In Wapenaar *et al.* (2011), a systematic comparison is given of SI methods, including ballistic MDD and crosscorrelation, for retrieving the reflection response from active and passive-source recordings. The passive SI methods are addressed for the case of transient-source recordings as well as for ambient noise recordings, which requires an adapted form in the case of the MDD application (van der Neut 2012). Here we focus only on the passive transient-source scenario, because this corresponds to earthquake recordings. We review the theory of ballistic MDD and crosscorrelation and introduce our new formulation for retrieving multicomponent reflection responses at the free surface.

2.1 Ballistic MDD

We formulate the reciprocity relation of the convolution type for a passive transient-source configuration to study the interaction quan-

tities of wavefields in two independent states, A and B (Wapenaar *et al.* 2008). The respective wavefields in each state are considered in the same arbitrary inhomogeneous anisotropic dissipative medium in which we define a domain $\mathbb{D}$ enclosed by a boundary $\partial\mathbb{D}$. We divide boundary $\partial\mathbb{D}$ into a horizontal part at the level of the acquisition array, defined by the receiver positions $\mathbf{x}_R \in \partial\mathbb{D}_R$, and an arbitrarily shaped part $\partial\mathbb{D}_M$ inside the medium (Fig. 1). Boundary $\partial\mathbb{D}_M$ has absorbing boundary conditions in both states A and B, while the boundary conditions of $\partial\mathbb{D}_R$ differ between states. The measurement state A represents the actual medium in which the passive wavefields can be recorded. This medium contains a free surface at the level of the acquisition array. Instead of a free surface, state B has absorbing boundary conditions at $\partial\mathbb{D}_R$. Hence, inside reference state B, fields do not have free-surface interaction and are denoted by the superscript 'o'. Sources in state A are introduced immediately below the boundary $\partial\mathbb{D}_R$ at positions $\mathbf{x}_A$. However, by invoking source–receiver reciprocity, sources at $\mathbf{x}_A$ function as receivers. In state B the source locations, $\mathbf{x}_B$, are anywhere inside the domain. Using these state definitions, the reciprocity theorem of the convolution type for acoustic wavefields in 3-D media yields a Fredholm integral of the first kind:

$$\int_{\partial\mathbb{D}_R} \hat{R}_{k|3}(\mathbf{x}_A, \mathbf{x}_R, \omega)\hat{P}^o(\mathbf{x}_R, \mathbf{x}_B, \omega)\mathrm{d}^2\mathbf{x}_R$$
$$= \hat{V}^o_k(\mathbf{x}_A, \mathbf{x}_B, \omega) - \hat{V}_k(\mathbf{x}_A, \mathbf{x}_B, \omega). \tag{1}$$

This relation is expressed in the space-frequency domain, where ω denotes the angular frequency. $\hat{R}_{k|3}(\mathbf{x}_A, \mathbf{x}_R, \omega)$ is the desired impulsive particle-velocity reflection response at $\mathbf{x}_A$ caused by a vertical-traction source at $\mathbf{x}_R$ at the free surface. This response is defined in the measurement state A with free surface and therefore contains free-surface multiples. The lower-case subscript on the left side of the vertical bar, with possible values 1, 2 or 3, denotes the receiver component of the field, while the subscript on the right side denotes the component of the virtual source. The kernel of the Fredholm integral, $\hat{P}^o(\mathbf{x}_R, \mathbf{x}_B, \omega)$, is the passive pressure-field response at $\mathbf{x}_R$ due to a source at $\mathbf{x}_B$ in the reference state without free surface. $\hat{V}_k(\mathbf{x}_A, \mathbf{x}_B, \omega)$ and $\hat{V}^o_k(\mathbf{x}_A, \mathbf{x}_B, \omega)$ represent the passive particle-velocity responses for the situation with and without free surface, respectively, at $\mathbf{x}_A$ due to a source at $\mathbf{x}_B$. The source at $\mathbf{x}_B$ does not require a subscript, because the relation holds for any kind of source mechanism. Note that $\hat{V}_k(\mathbf{x}_A, \mathbf{x}_B, \omega)$ represents the actual measurements, from which $\hat{V}^o_k(\mathbf{x}_A, \mathbf{x}_B, \omega)$ and the kernel, $\hat{P}^o(\mathbf{x}_R, \mathbf{x}_B, \omega)$, need to be extracted. The integral boundary is defined by the receiver positions of the passive measurements at the horizontal acquisition level $\partial\mathbb{D}_R$. We let the remaining part of the closed boundary, $\partial\mathbb{D}_M$, extend to infinity such that its contribution to the integral vanishes due to Sommerfeld's radiation condition. Note that the multiplication inside the integrand represents a convolution in the time domain. In order to solve for the reflection response, $\hat{R}_{k|3}(\mathbf{x}_A, \mathbf{x}_R, \omega)$, we need to invert eq. (1). However, in case we only have the recordings of a single passive source in a 2-D or 3-D medium, this inverse problem is severely ill-posed (Arfken & Weber 2005). We can constrain the problem by taking into account many passive source recordings. Employing the wavefield matrix notation (Berkhout 1982), eq. (1) becomes:

$$\hat{\mathbf{R}}_{k|3}\hat{\mathbf{P}}^o = \hat{\mathbf{V}}^o_k - \hat{\mathbf{V}}_k, \tag{2}$$

where boldface symbolizes the matrix form of the wavefields. A field matrix ($\hat{\mathbf{P}}^o$, $\hat{\mathbf{V}}^o_k$ and $\hat{\mathbf{V}}_k$) contains the independent non-overlapping recordings of passive sources, whereby each row represents a receiver position and each column a passive source in the
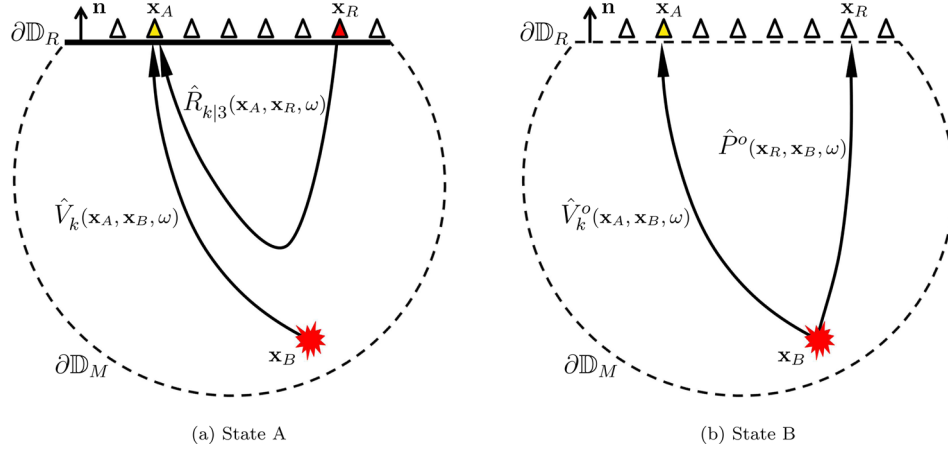
Figure 1. State definitions for ballistic MDD. (a) State A in the medium with free surface: the boundary of the domain, $\partial \mathbb{D}$, consists of a half-sphere, $\partial \mathbb{D}_M$, with infinite radius and a horizontal free surface (thick continuous line), $\partial \mathbb{D}_R$, with normal vector **n**. The receivers at boundary $\partial \mathbb{D}_R$ are denoted by triangles: red indicates the position of the virtual source and yellow its corresponding receiver. $\hat{R}_{k|3}(\mathbf{x}_A, \mathbf{x}_R)$ is the reflection response at $\mathbf{x}_A$ to a virtual vertical traction source at $\mathbf{x}_R$ and contains free-surface multiples. $\hat{V}_k(\mathbf{x}_A, \mathbf{x}_B, \omega)$ is the particle-velocity response at receiver position $\mathbf{x}_A$ due to an arbitrary passive source at $\mathbf{x}_B$ (red star) and contains free-surface multiples. (b) State B in the medium without free surface: here the acquisition boundary $\partial \mathbb{D}_R$ has absorbing boundary conditions (dotted line). $\hat{P}^o(\mathbf{x}_R, \mathbf{x}_B, \omega)$ and $\hat{V}_k^o(\mathbf{x}_A, \mathbf{x}_B, \omega)$ are the pressure response at $\mathbf{x}_R$ and particle-velocity response at $\mathbf{x}_A$, respectively, due to an arbitrary passive source at $\mathbf{x}_B$ (red star).

subsurface. The reflection response $\hat{\mathbf{R}}_{k|3}$ is similar, except that it is a square matrix and its columns correspond to independent virtual sources at the surface. The normal form (van der Neut *et al.* 2011) of eq. (2) for the particle-velocity reflection response is given by

$$\hat{\mathbf{R}}_{k|3} \hat{\mathbf{P}}^o \hat{\mathbf{P}}^{o\dagger} = \left(\hat{\mathbf{V}}_k^o - \hat{\mathbf{V}}_k \right) \hat{\mathbf{P}}^{o\dagger}, \tag{3}$$

where † denotes transposition and complex conjugation. To solve for the unknown reflection response we implement regularized least-squares inversion:

$$\hat{\mathbf{R}}_{k|3} = \left[\left(\hat{\mathbf{V}}_k^o - \hat{\mathbf{V}}_k \right) \hat{\mathbf{P}}^{o\dagger} \right] \left[\hat{\mathbf{P}}^o \hat{\mathbf{P}}^{o\dagger} + \epsilon^2 \mathbf{I} \right]^{-1}, \tag{4}$$

where the first term in square brackets on the right-hand side represents the 'correlation function', while the second term in square brackets is the inverse matrix: it contains the 'point-spread function' (PSF) and the regularization matrix, which is composed of a stabilization parameter, ϵ^2, and the identity matrix **I** (van der Neut 2012). This operation represents an MDD, which implies that the reflection response is retrieved for all virtual sources and receivers simultaneously. This makes MDD distinctly different from Green's function retrieval by crosscorrelation, which obtains the response independently for each virtual-source position. The reference-state fields without free-surface interaction, $\hat{\mathbf{P}}^o$ and $\hat{\mathbf{V}}_k^o$, could be obtained by removing all surface-related multiples from the passive recordings, but in practice this is an extremely challenging procedure. Therefore, we estimate the field $\hat{\mathbf{V}}_k^o$ by extracting the only event we can distinguish from other events with considerable certainty: the direct arrival of the passive recording $\hat{\mathbf{V}}_k$ (which can include possible short-period multiples). We multiply the direct arrival by a factor $\frac{1}{2}$ to account for the absence of the free surface in the reference state. This estimate is quite reliable for the implementation of MDD when the medium is weakly scattering. Since measurements are usually obtained at the free surface, $\hat{\mathbf{P}}^o$ can be estimated from the vertical particle-velocity recordings by an additional far-field approximation: $\hat{P}^o \approx -\rho c \hat{V}_3^o$, where ρ and c are the mass density and *P*-wave velocity, respectively, at the receiver locations. eq. (4) thus becomes:

$$\hat{\mathbf{R}}_{k|3} \approx \frac{1}{\rho c} \left[\left(\hat{\mathbf{V}}_k - \hat{\mathbf{V}}_k^D \right) \hat{\mathbf{V}}_3^{D\dagger} \right] \left[\hat{\mathbf{V}}_3^D \hat{\mathbf{V}}_3^{D\dagger} + \epsilon^2 \mathbf{I} \right]^{-1}, \tag{5}$$

where the superscript '*D*' indicates that the wavefield is the direct wave of the particle-velocity recording multiplied by the factor $\frac{1}{2}$. Note that the ϵ in this equation is a scaled version of the ϵ in eq. (4). The direct-wave approximation will cause errors in both the correlation function and the inverse matrix, which inevitably propagate into the solution $\hat{\mathbf{R}}_{k|3}$. Physically speaking, this approximation means that the PSF in the inverse matrix, $\hat{\mathbf{V}}_3^D \hat{\mathbf{V}}_3^{D\dagger}$, is now only constructed by the direct incident wavefield of the passive particle-velocity recordings: the ballistic wavefield. This is why we have designated this MDD method as 'ballistic MDD'. The fact that the PSF is estimated by ballistic wavefields limits this MDD method to use only the wavenumbers provided directly by the passive-source distribution. Moreover, the ballistic PSF can only correct for anisotropy in the virtual-source radiation patterns caused by irregular source distributions and mechanisms, but not for anisotropy resulting from scattering inside the medium.

An approximation to the reflection response $\hat{R}_{k|3}$ can alternatively be obtained from the reciprocity relation of the correlation type, as presented in Wapenaar & Fokkema (2006):

$$\Re \left[\hat{R}_{k|3}(\mathbf{x}_A, \mathbf{x}_R, \omega) \right] \langle \hat{S}(\omega) \rangle$$

$$\approx \int_{\partial \mathbb{D}_S} \rho(\mathbf{x}_B) c(\mathbf{x}_B) \hat{V}_3^*(\mathbf{x}_R, \mathbf{x}_B, \omega) \hat{V}_k(\mathbf{x}_A, \mathbf{x}_B, \omega) \mathrm{d}^2 \mathbf{x}_B. \tag{6}$$

The integral is along the distribution of passive sources at locations $\mathbf{x}_B \in \partial \mathbb{D}_S$ in the subsurface, where $\rho(\mathbf{x}_B)$ and $c(\mathbf{x}_B)$ denote the mass density and *P*-wave velocity of the medium, respectively, at these same locations. $\hat{V}_3(\mathbf{x}_R, \mathbf{x}_B, \omega)$ and $\hat{V}_k(\mathbf{x}_A, \mathbf{x}_B, \omega)$ are particle-velocity recordings at receiver positions $\mathbf{x}_R$ and $\mathbf{x}_A$, respectively, due to a passive source at $\mathbf{x}_B$. Note that superscript '*' denotes complex conjugation, which implies that the integrand product represents a crosscorrelation in the time-domain. The left-hand side denotes the causal and the acausal impulsive particle-velocity reflection response at receiver $\mathbf{x}_A$ due to a vertical-traction source at $\mathbf{x}_R$. $\langle \hat{S}(\omega) \rangle$ is the average power spectrum of the passive sources. Although eq. (6) retrieves the same response as eq. (1), their underlying solution methods differ significantly. Eq. (6) is solved explicitly, which explains the relative robustness of the method. However, due

(a) State A   (b) State B
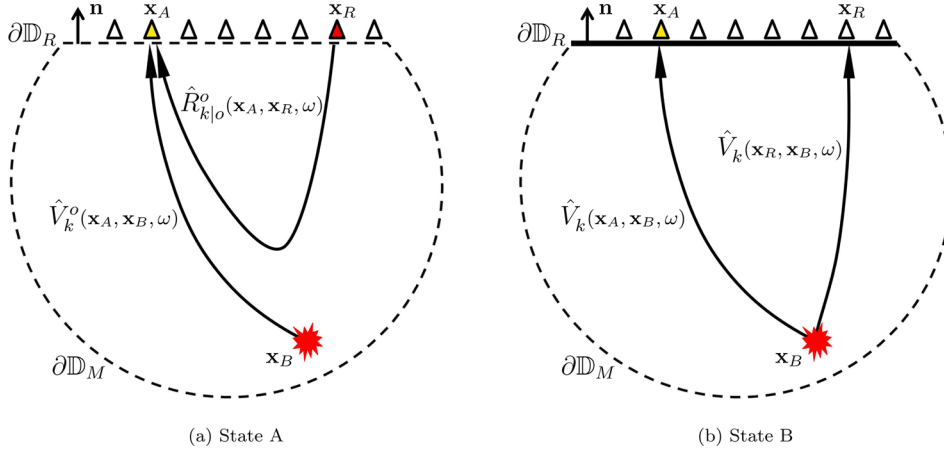
Figure 2. State definitions for full-field MDD. (a) State A in the medium without free surface: the boundary of the domain, $\partial\mathbb{D}$, consists of a half-sphere, $\partial\mathbb{D}_M$, with infinite radius and a horizontal surface, $\partial\mathbb{D}_R$, with normal vector $\mathbf{n}$. The receivers at boundary $\partial\mathbb{D}_R$ are denoted by triangles: red indicates the position of the virtual source and yellow its corresponding receiver. $\hat{R}^o_{k|0}(\mathbf{x}_A, \mathbf{x}_R, \omega)$ is the reflection response at $\mathbf{x}_A$ to a monopole virtual source at $\mathbf{x}_R$ and is without free-surface multiples. $\hat{V}^o_k(\mathbf{x}_A, \mathbf{x}_B, \omega)$ is the particle-velocity response at receiver position $\mathbf{x}_A$ due to an arbitrary passive source at $\mathbf{x}_B$ (red star) without free-surface multiples. (b) State B in the medium with free surface: here the acquisition boundary $\partial\mathbb{D}_R$ forms a free surface (thick continuous line). $\hat{V}_k(\mathbf{x}_R, \mathbf{x}_B, \omega)$ and $\hat{V}_k(\mathbf{x}_A, \mathbf{x}_B, \omega)$ are the particle-velocity responses with free-surface multiples at $\mathbf{x}_R$ and $\mathbf{x}_A$, respectively, due to an arbitrary passive source at $\mathbf{x}_B$ (red star).

to the formulation of the integral, it does require a well-sampled enclosing boundary of passive sources: a condition unlikely to be met by earthquake sources, which are generally sparse. Eq. (1) is implicit and hence requires inversion. However, a concomitant advantage of inversion is that it corrects for the imprint of the irregular passive-source illumination. Moreover, since the integral of eq. (1) is along the positions of the receivers instead of the passive sources, it still works when the source distribution is sparse, as long as the receivers form a well-sampled and sufficiently extended array.

2.2 Full-field MDD

We now introduce our formulation for the alternative MDD method, which uses both the ballistic and coda (or scattered) wavefield of the data: the full field. We use the same setting as for ballistic MDD, but we change the boundary conditions: we appoint state B as the measurement state with free surface, while state A is the reference state without free surface (denoted by superscript 'o') of which we aim to determine the reflection response (Fig. 2). This switch of the boundary conditions at $\partial\mathbb{D}_R$ between states ensures that the kernel now contains the measured data (which avoids the need to extract the direct wave to build the kernel) and allows us to retrieve a reflection response without free-surface multiples. Note that the source locations $\mathbf{x}_A$ and $\mathbf{x}_B$ remain the same as for ballistic MDD. The acoustic representation in 3-D media is presented in the space-frequency domain as

$$\int_{\partial\mathbb{D}_R} \hat{R}^o_{k|0}(\mathbf{x}_A, \mathbf{x}_R, \omega)\hat{V}_3(\mathbf{x}_R, \mathbf{x}_B, \omega)\mathrm{d}^2\mathbf{x}_R$$

$$= \hat{V}_k(\mathbf{x}_A, \mathbf{x}_B, \omega) - \hat{V}^o_k(\mathbf{x}_A, \mathbf{x}_B, \omega). \qquad (7)$$

For the derivation in elastic 3-D media, refer to Appendix A. Note that in this formulation the unknown particle-velocity reflection response $\hat{R}^o_{k|0}$ is caused by a monopole source and does not contain free-surface multiples. The monopole source is indicated by subscript zero '0', because it is a scalar. The kernel, $\hat{V}_3(\mathbf{x}_R, \mathbf{x}_B, \omega)$, is the full recording of the vertical particle-velocity at receiver $\mathbf{x}_R$ at the free surface of the actual medium due to an arbitrary passive

source at $\mathbf{x}_B$. The source type, signature and location of the passive sources at $\mathbf{x}_B$ do not need to be known. Similar to eq. (1), this equation is a Fredholm integral of the first kind, but with a different solution $\hat{R}^o_{k|0}(\mathbf{x}_A, \mathbf{x}_R, \omega)$ and a kernel which does not require approximations. eq. (7) presents an inverse problem, which also requires to be constrained by considering many passive source recordings. We express eq. (7) using wavefield matrix notation:

$$\hat{\mathbf{R}}^o_{k|0}\hat{\mathbf{V}}_3 = \hat{\mathbf{V}}_k - \hat{\mathbf{V}}^o_k. \qquad (8)$$

The normal form of eq. (8) for the particle-velocity reflection response is given by

$$\hat{\mathbf{R}}^o_{k|0}\hat{\mathbf{V}}_3\hat{\mathbf{V}}^\dagger_3 = \left(\hat{\mathbf{V}}_k - \hat{\mathbf{V}}^o_k\right)\hat{\mathbf{V}}^\dagger_3, \qquad (9)$$

and we solve by regularized least-squares

$$\hat{\mathbf{R}}^o_{k|0} = \left[\left(\hat{\mathbf{V}}_k - \hat{\mathbf{V}}^o_k\right)\hat{\mathbf{V}}^\dagger_3\right]\left[\hat{\mathbf{V}}_3\hat{\mathbf{V}}^\dagger_3 + \epsilon^2\mathbf{I}\right]^{-1}. \qquad (10)$$

Note that in this case, the evaluation of the PSF in the regularized inverse matrix does not require any approximations: it is constructed by the full recordings of the particle-velocity response of the medium. Hence, we refer to this MDD method as 'full-field MDD'. The term 'full-field' originates from the fact that the PSF is constructed by the full passive recordings, containing both the ballistic and the coda wavefields. Note that this means that this MDD effectively uses the wavenumbers provided by the ballistic as well as all scattered events in the data (this includes the free-surface multiples). Therefore, this full-field PSF also corrects for anisotropic illumination caused by both the ballistic field and the scattering inside the medium.

In order to solve for the reflection response in eq. (10), $\hat{\mathbf{V}}^o_k$ in the right-hand side needs to be estimated in the same way as we did for eq. (5): by extracting the direct field from each passive recording and multiply by a factor $\frac{1}{2}$. However, we do not require the additional far-field approximation here. The equation thus becomes:

$$\hat{\mathbf{R}}^o_{k|0} \approx \left[\left(\hat{\mathbf{V}}_k - \hat{\mathbf{V}}^D_k\right)\hat{\mathbf{V}}^\dagger_3\right]\left[\hat{\mathbf{V}}_3\hat{\mathbf{V}}^\dagger_3 + \epsilon^2\mathbf{I}\right]^{-1}. \qquad (11)$$

It is important to remark that in the case of full-field MDD the direct-wave approximation only occurs in the correlation function. The wavefields in the PSF however, do not require any approximations.

We have discussed two essentially different MDD methods. Ballistic MDD retrieves the reflection response with free-surface multiples, while full-field MDD retrieves the response without free-surface multiples. The kernel of the latter is constructed by the full passive data and thus governs a wide spectrum of wavenumbers, while the kernel of the former is limited to the wavenumbers of the passive ballistic field. As a consequence, the full-field PSF takes into account additional wavenumber illumination provided by the recorded scattered field and consequently corrects for the irregular illumination it may cause. These points lead us to hypothesize that full-field MDD applies a better constrained inversion and yields a more accurate retrieval of the reflection response than ballistic MDD. Nevertheless, we still expect the retrieval of the reflection response to be contaminated by some artefacts, since the correlation function of full-field MDD does contain the approximated $\hat{\mathbf{V}}_k^D$ field.

3 NUMERICAL RESULTS

We conduct an effective comparison of retrieving the particle-velocity reflection response by crosscorrelation (eq. 6), ballistic MDD (eq. 5) and full-field MDD (eq. 11). Here we choose to analyse only the vertical-component particle-velocity reflection response by setting subscript k to 3, but we emphasize that we can equally well obtain the horizontal components when the input data provides them. To simulate the input recordings, we perform independent 2-D numerical experiments using acoustic finite-difference wavefield simulation (Thorbecke & Draganov 2011). We use a lithospheric model with a Moho reflector at 50 km depth with a discontinuity, which is characterized by a downward vertical displacement of 10 km (Fig. 3a). The *P*-wave velocities of the crust and upper mantle are 6 and 9 km s^{-1}, respectively, and the respective densities are 2700 and 3400 kg m^{-3} (Dziewonski & Anderson 1981). We generate independent passive recordings by modelling dipole sources which we orient approximately tangential to the alignment of the source locations, with some random directional deviation. This has the purpose to approximate the effect of slip occurring along an irregular listric fault system. For each passive-source signature we use a different Ricker wavelet with a peak frequency varying between 0.3 and 1.1 Hz. In Fig. 3(a), the orientation and location of the passive dipole sources are indicated by arrows: the colour defines their peak frequency. The 200 multicomponent receivers are placed 0.2 km beneath the free surface with an inter-receiver spacing of 1 km. However, the receivers can be considered to be approximately at the free-surface level, because 0.2 km is less than 4 per cent of the smallest central wavelength in the upper layer. We model the passive recordings for a total time of 170 s to ensure that free-surface multiples of higher orders are present in the data.

3.1 Different illumination scenarios

We conduct the comparison for two different irregular source distributions: the first provides full coverage (Fig. 3a), while the second provides only limited illumination from the sides (Fig. 4a).

3.1.1 Complete illumination

We use the three interferometric methods to retrieve a reflection response to a virtual source at the position of the middle receiver (position 0 km) for the case of sufficient passive-source illumination (Fig. 3). To enable a visual analysis of the quality of the retrieved reflection responses, we directly model the reflection response by placing a monopole source at the position of the middle receiver with a peak frequency of 1.1 Hz, depicted in Fig. 3(b). This modelled response is characterized by four distinct events: the direct wave, the primary Moho reflection, the diffraction of the Moho discontinuity and the first free-surface multiple reflection. We focus on the body-wave reflections: the primary and the first free-surface multiple, which at position 0 km have two-way traveltimes of approximately 17 and 34 s, respectively. The visible jump in the body-wave reflections and the corresponding diffractions are caused by the Moho discontinuity.

We first compare the reflection retrieved by crosscorrelation in Fig. 3(c) to the modelled response in Fig. 3(b). The resolution of the crosscorrelation result is significantly lower, which makes it difficult to distinguish the primary or the free-surface multiple reflection. This low resolution is caused by the variation in spectra between individual passive sources. In spite of the low resolution, the primary reflection can be distinguished at positions −100 to −50 km and 50 to 100 km. Between positions −50 and 50 km, the primary reflection becomes more obscured by the presence of artefacts, which makes it difficult to detect the Moho discontinuity. The artefacts are a result of the anisotropic illumination of the array due to the variations in passive-source radiation patterns.

The result of ballistic MDD is shown in Fig. 3(d). The resolution of this reflection retrieval is comparable to the modelled response in Fig. 3(b). The primary is retrieved for each receiver position and it is possible to detect the jump caused by the Moho discontinuity. However, the primary is not very distinct, because its amplitude is not significantly higher than most of the artefacts. At about 4 s after the primary an erroneous 'ghost' of the primary is clearly visible, which, in the realistic case when the medium parameters are not known, could result in an incorrect interpretation of a reflectivity contrast. This interferometric ghost is caused by crosscorrelations between direct waves and primaries in the correlation function. The ballistic PSF cannot correct for this, because it only contains the spectral information of the direct waves (see Fig. 5a). In addition to this predominant artefact, the retrieved primary reflection is slightly obscured by steep-dipping artefacts around the centre of the array, near position 0 km. The free-surface multiple is significantly weaker than in the modelled response. This is not in accordance with the theory, which states that ballistic MDD retrieves the reflection response with free-surface interaction.

In Fig. 3(e) the reflection response retrieved by full-field MDD is shown. The resolution is of the same quality as the modelled reflection response. The primary reflection is retrieved completely and is distinctly stronger than the artefacts in the background. However, there is a slight decrease in amplitude at lower angles of incidence. The free-surface multiple is expected to be absent, but we can still see some remnants of it. The diffraction caused by the upper corner of the Moho discontinuity is, though obscured by artefacts, partially retrieved by full-field MDD.

When we compare results of ballistic and full-field MDD, we see that the latter gives a more distinct reflection response and is not as obscured by artefacts as the former. Full-field MDD does not contain the erroneous primary ghost we see in the result of ballistic MDD. This indicates that the full-field PSF is more effective in correcting for artefacts (see Fig. 5b). Moreover, ballistic MDD required a stabilization parameter two orders of magnitude larger than full-field MDD.
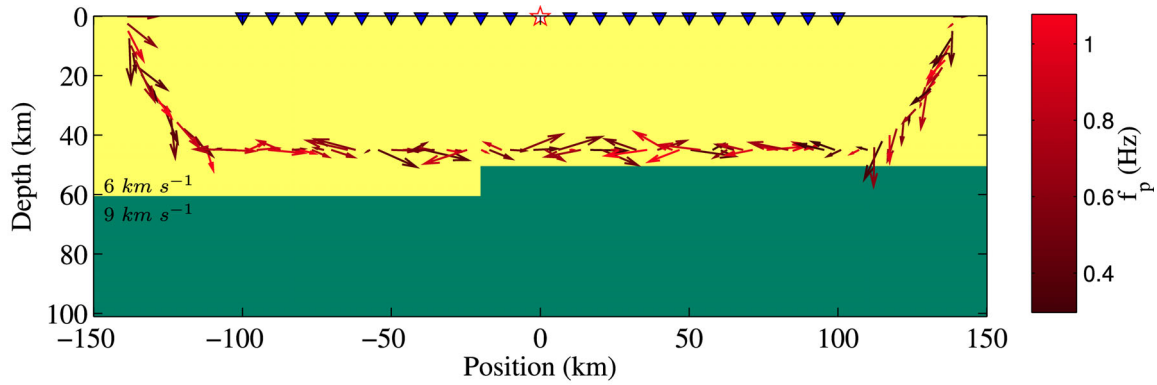
(a) Model
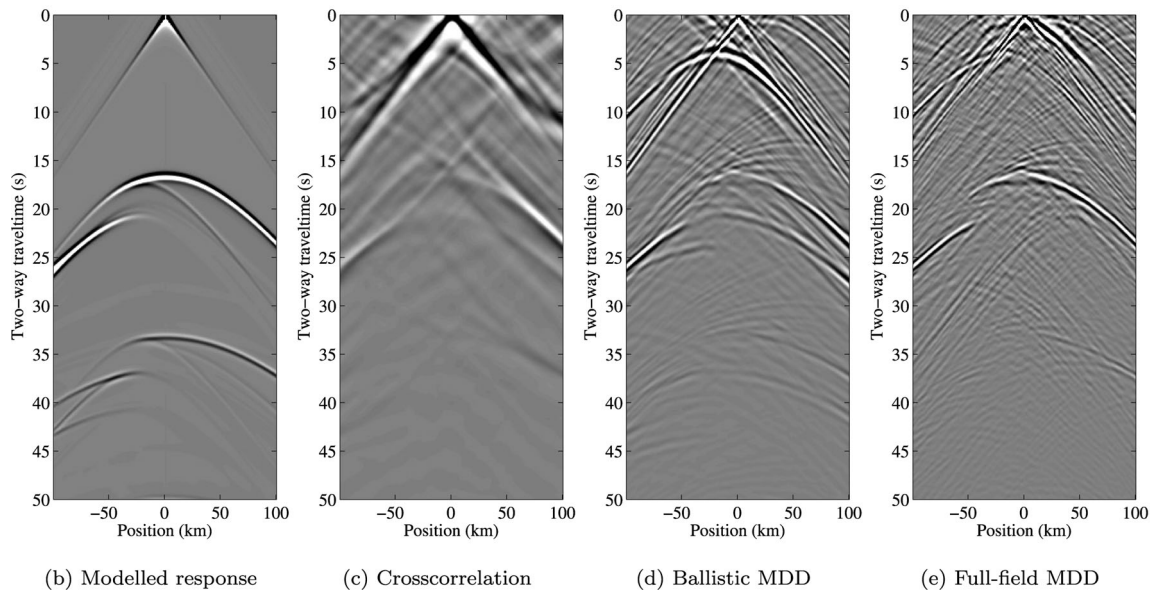
(b) Modelled response   (c) Crosscorrelation   (d) Ballistic MDD   (e) Full-field MDD

Figure 3. Complete illumination scenario. (a) *P*-wave speed model (km s^{-1}) for the complete illumination scenario. The orientation and location of the passive dipole sources are denoted by arrows and the receivers by blue triangles. The colour of the arrows indicates the peak frequency (f_p) of the passive-source signatures as specified by the colour bar. The position along the horizontal axis corresponds with the horizontal axis of the modelled and retrieved shot gathers. (b) Modelled vertical particle-velocity reflection response to a vertical dipole-source placed at the position of the middle receiver. (c) Vertical particle-velocity reflection response obtained by crosscorrelation. (d) Vertical particle-velocity reflection response obtained by ballistic MDD. (e) Vertical particle-velocity reflection response obtained by full-field MDD.

3.1.2 Limited illumination

In Fig. 4 we compare all three interferometric methods for the case of having passive sources positioned at the far sides of the model. In this challenging configuration, low-angle reflections at the centre of the array can only be retrieved from diffractions and multiply scattered waves contained in the coda field of the input recordings.

The crosscorrelation result in this illumination scenario differs from the complete illumination case (Fig. 3c) in that it does not show any sign of the Moho primary between positions −50 and 50 km (Fig. 4c). This implies that for this situation, crosscorrelation only profits effectively from first order and not from higher order multiples, because only the latter could yield a retrieval of the Moho reflection at the positions between −50 and 50 km. This makes it impossible to detect the Moho discontinuity.

In Fig. 4(d) the ballistic MDD result is shown, which is severely contaminated by artefacts and does not show a reflection retrieval. These artefacts are caused by the ballistic PSF, which is designed

to correct for irregularities in virtual shot gathers which are entirely retrieved from the ballistic passive field, which is here constructed from high-angle events only (see Fig. 5c). However, in this scenario, the retrieved virtual reflections can only be constructed from the scattered events contained in the passive recordings and thus the ballistic PSF will only introduce artefacts.

Fig. 4(e) shows that full-field MDD does yield a visible reflection for all receiver positions. This is due to the fact that full-field MDD uses diffractions and multiples of different orders, contained in the coda field, to construct the reflection response for all available wavenumbers. The full-field PSF is designed to correct for illumination irregularities caused by both the ballistic and the coda wavefield (see Fig. 5d). However, there is a notable decrease in amplitude for the lower wavenumbers, which makes it slightly more difficult to distinguish the primary from artefacts when compared to the case of complete illumination in Fig. 3(e). In spite of this, full-field MDD is the only method which can still obtain a reflection response under these severely limited illumination conditions
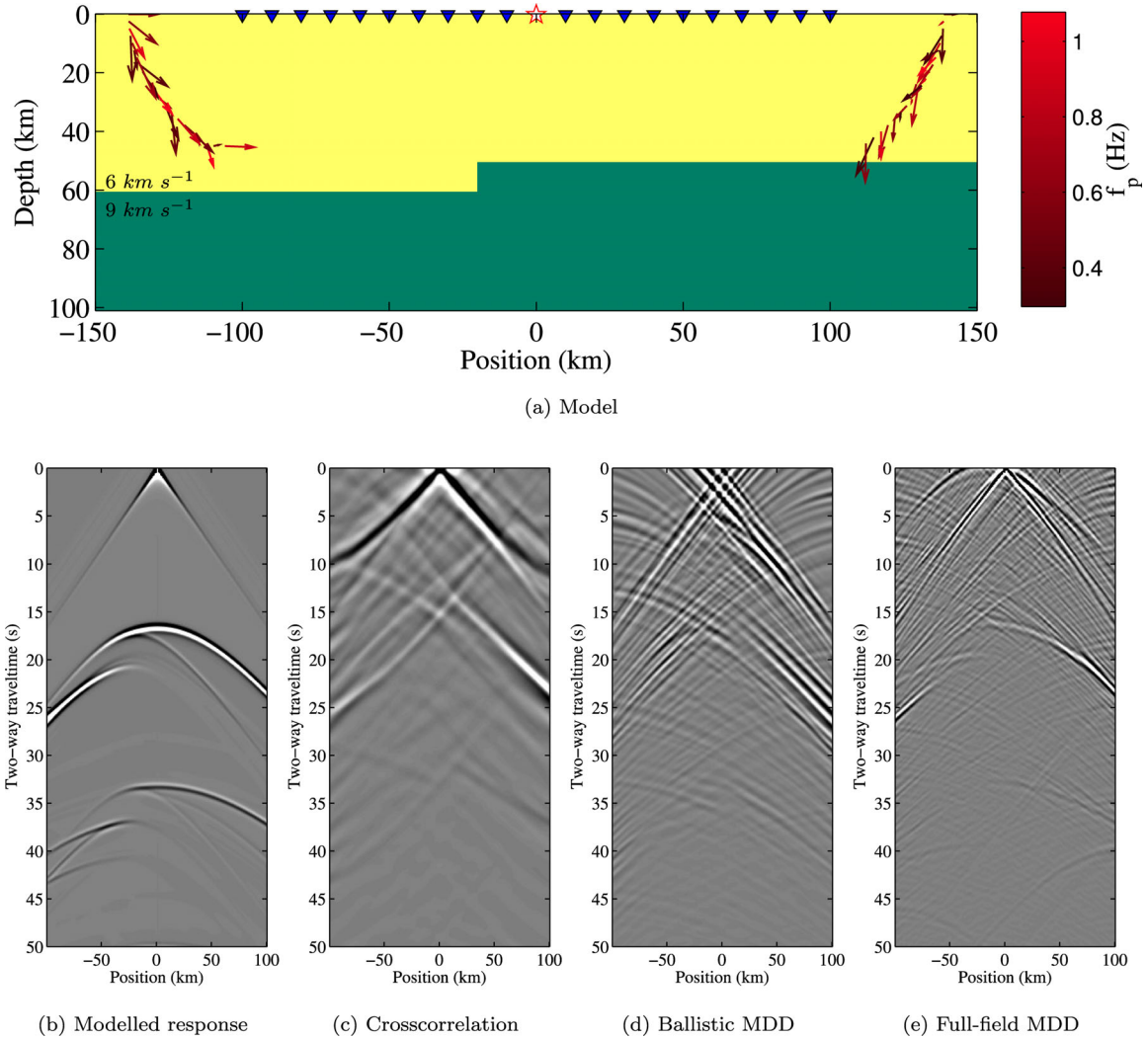
(a) Model

(b) Modelled response   (c) Crosscorrelation   (d) Ballistic MDD   (e) Full-field MDD

Figure 4. Same as in Fig. 3, but for limited illumination (high angles only).

and allows for a reasonably accurate interpretation of the Moho discontinuity.

3.2 PSF analysis

Conventionally, the function of the PSF is to properly balance the virtual-shot gathers, such that each virtual source resembles an isotropic source mechanism. From the theory, as well as the numerical results, we have learned that the ballistic PSF achieves this by balancing the irregular illumination caused by the directly incident passive wavefields. On the other hand, the full-field PSF balances the irregular illumination associated with the full passive recording and additionally uses the scattered passive events to convert free surface multiples into primaries in the resulting reflection response. To gain insight into the differences in illumination characteristics, we compare the full-field and ballistic PSF in the time-space and frequency-wavenumber domains.
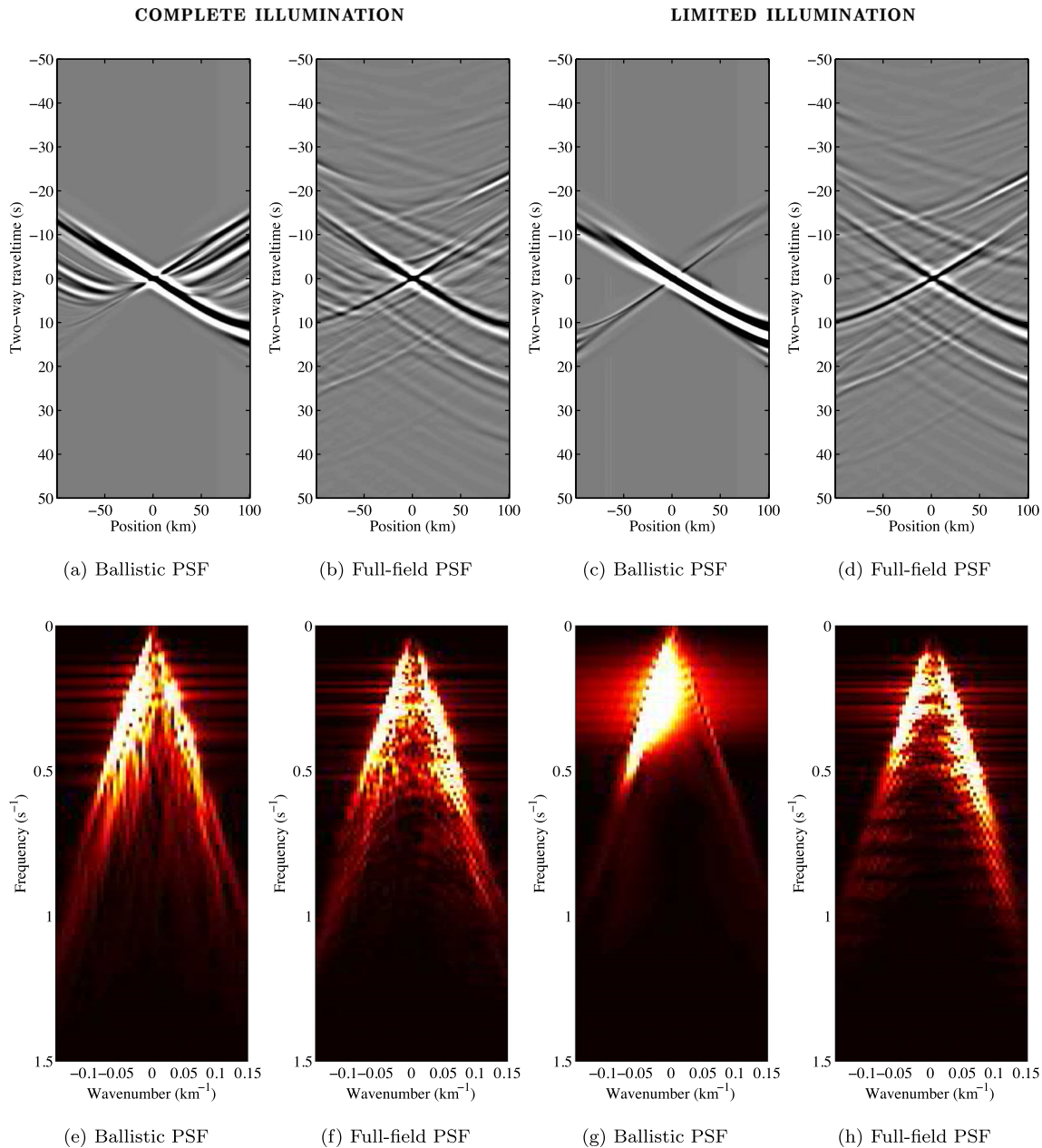
First, the time–space plots in Figs 5(a) and (c) show that the ballistic PSF is constructed of the directly incident fields only, while Figs 5(b) and (d) show that the full-field PSF includes all scattered events as well. Note that the apparent difference between the full-field PSF in the case of complete and limited illumination is not significant. The frequency–wavenumber spectrum of the ballistic

PSF (Fig. 5e) shows that for complete illumination (Fig. 3a), the ballistic fields provide a broad range of wavenumbers. This is in stark contrast with the case of limited illumination from the sides (Fig. 4a), where the ballistic fields of the passive sources only provide high wavenumbers (Fig. 5g). Moreover, the application of the tapered time-window for selecting the ballistic fields causes smearing, which introduces artificial low wavenumbers between 0.1 and 0.4 Hz.

Figs 5(f) and (h) show the corresponding full-field PSF's for the two illumination scenarios, which appear to be similar in spectral content even though the directional balancing is different for each scenario. In both cases, the full-field PSF clearly displays distinct features which indicate the presence of spectral information due to the coda wavefield, which is necessary to balance the virtual-source radiation and is responsible for converting free-surface multiples into primaries.

3.3 Direct-wave approximation sensitivity

Eqs (5) and (11) both rely on the direct wave to approximate the reference-state response to the passive sources. This approximation will inevitably cause errors in retrieved reflections. To analyse this error, we additionally compute the reflection retrievals using

COMPLETE ILLUMINATION   **LIMITED ILLUMINATION**

(a) Ballistic PSF   (b) Full-field PSF   (c) Ballistic PSF   (d) Full-field PSF

(e) Ballistic PSF   (f) Full-field PSF   (g) Ballistic PSF   (h) Full-field PSF

Figure 5. Ballistic and full-field PSF's of the virtual source at position 0 km for the complete (Fig. 3a) and limited (Fig. 4a) illumination scenarios. (a) Ballistic PSF in the *t–x* domain for complete illumination. (b) Full-field PSF in the *t–x* domain for complete illumination. (c) Ballistic PSF in the *t–x* domain for limited illumination. (d) Full-field PSF in the *t–x* domain for limited illumination. (e)–(h) show the *f–k* spectra of (a)–(d).

eqs (4) and (10), which are without the direct-wave approximation. This required numerical simulation of the actual reference-state responses by using the model setting in Fig. 3(a) with absorbing boundary conditions at the top. This allows us to compare reflection responses obtained using the direct-wave approximation (eqs 5 and 11) and without using the direct-wave approximation (eqs 4 and 10).

Figs 6(a) and (b) show the reflection response retrieved by ballistic MDD using eqs (5) and (4), respectively. In the result without approximation in Fig. 6(b), the primary is more distinct and continuous and the source ghost is less visible, compared to the result obtained using the direct-wave approximation in Fig. 6(a). The free-surface multiple is clearly more visible in Fig. 6(b), which is in accordance with the theory which states that ballistic

MDD retrieves the response with free-surface interaction. Figs 6(c) and (d) display the results for full-field MDD with (eq. 11) and without using the direct-wave approximation (eq. 10), respectively. The free-surface multiple is suppressed in both figures (although some remnants are still visible), which agrees with the fact that full-field MDD retrieves the reflection response without free-surface interaction. Note that the two results for full-field MDD do not differ much from each other, although artefacts are less apparent in Fig. 6(d).

This comparison shows that ballistic MDD is more affected by the direct-wave approximation than full-field MDD, which could be predicted when comparing eqs (5) and (11): the ballistic PSF requires the direct-wave approximation while the full-field PSF does not.

(a) Ballistic MDD, eq (5)   (b) Ballistic MDD, eq (4)   (c) Full-field MDD, eq (11)   (d) Full-field MDD, eq (10)
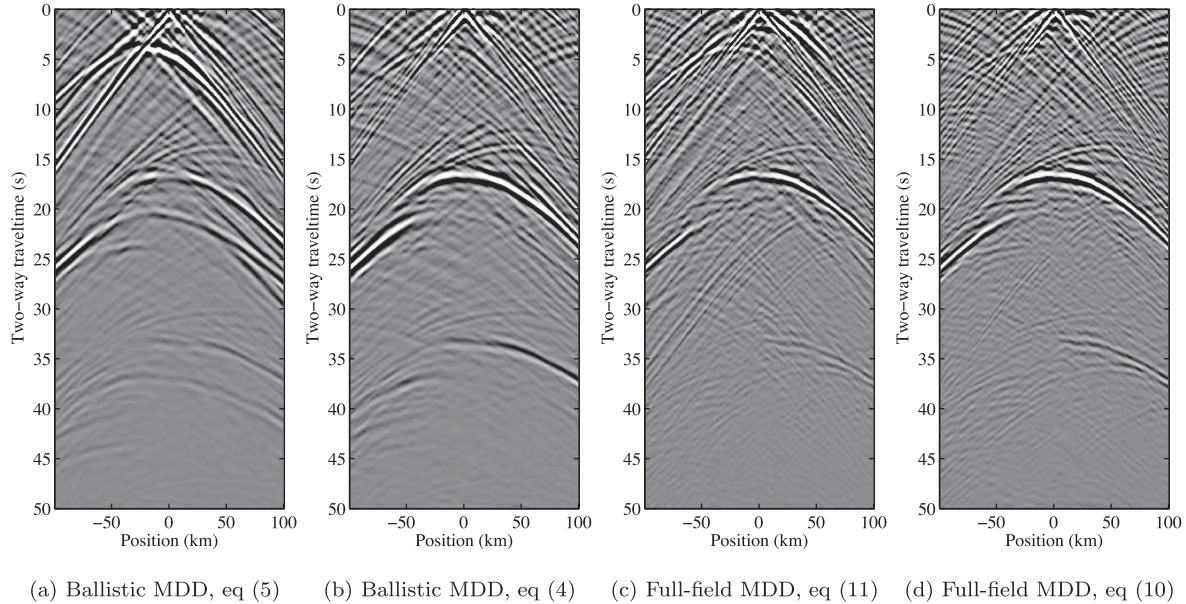
Figure 6. MDD methods with and without direct-wave approximation, for the complete illumination scenario described by Fig. 3(a). (a) Vertical particle-velocity reflection response using ballistic MDD with direct-wave approximation. (b) Idem, using ballistic MDD formulation with modelled reference responses. (c) Idem, using full-field MDD with direct-wave approximation. (d) Idem, using full-field MDD formulation with modelled reference responses.

3.4 Noise sensitivity

In order to create a more realistic scenario, we introduce noise in the modelled passive recordings. We generate random noise in the frequency-domain which is different for every shot and trace and we band-limit it between 0.01 and 2.6 Hz (see Fig. 7c). In Fig. 7(b) the effect of adding the noise can be seen in a trace at position 0 km of a passive-source recording. The primary, indicated by 'P', is easily recognizable in the trace contaminated by noise, but the first order free-surface multiple, indicated by 'M1', is below the noise level. This indicates that the ballistic field is not affected much by the noise, while the scattered events of the coda wavefield are. In the example of one of the passive-source recordings in Fig. 7(a) the effect of the noise is clearly visible: the free-surface multiples of higher order are obscured.

We compare the retrieved vertical particle-velocity reflection responses, using the three SI methods for the case of limited illumination, as shown in Fig. 4(a). The retrieved response by crosscorrelation is unaffected by the introduction of noise (Fig. 7e): the method diminishes incoherent or random events present in the input recordings. Ballistic and full-field MDD are much more affected by the noise (Figs 7f and g, respectively). This is because inversion is sensitive to the prevalence of noise. We partially compensated for this by increasing the stabilization parameter for full-field MDD to the same magnitude as used for ballistic MDD. Additional artefacts now contaminate the reflection response retrieved by ballistic MDD even more (Fig. 7f). In Fig. 7(g) it can be seen that the noise introduces a random pattern in the response retrieved by full-field MDD. However, the accuracy and visibility of the reflection response is not significantly affected with respect to Fig. 4(e). Moreover, the noise-related artefacts could be minimized by making use of sparsity promotion as presented by van der Neut & Herrmann (2013).
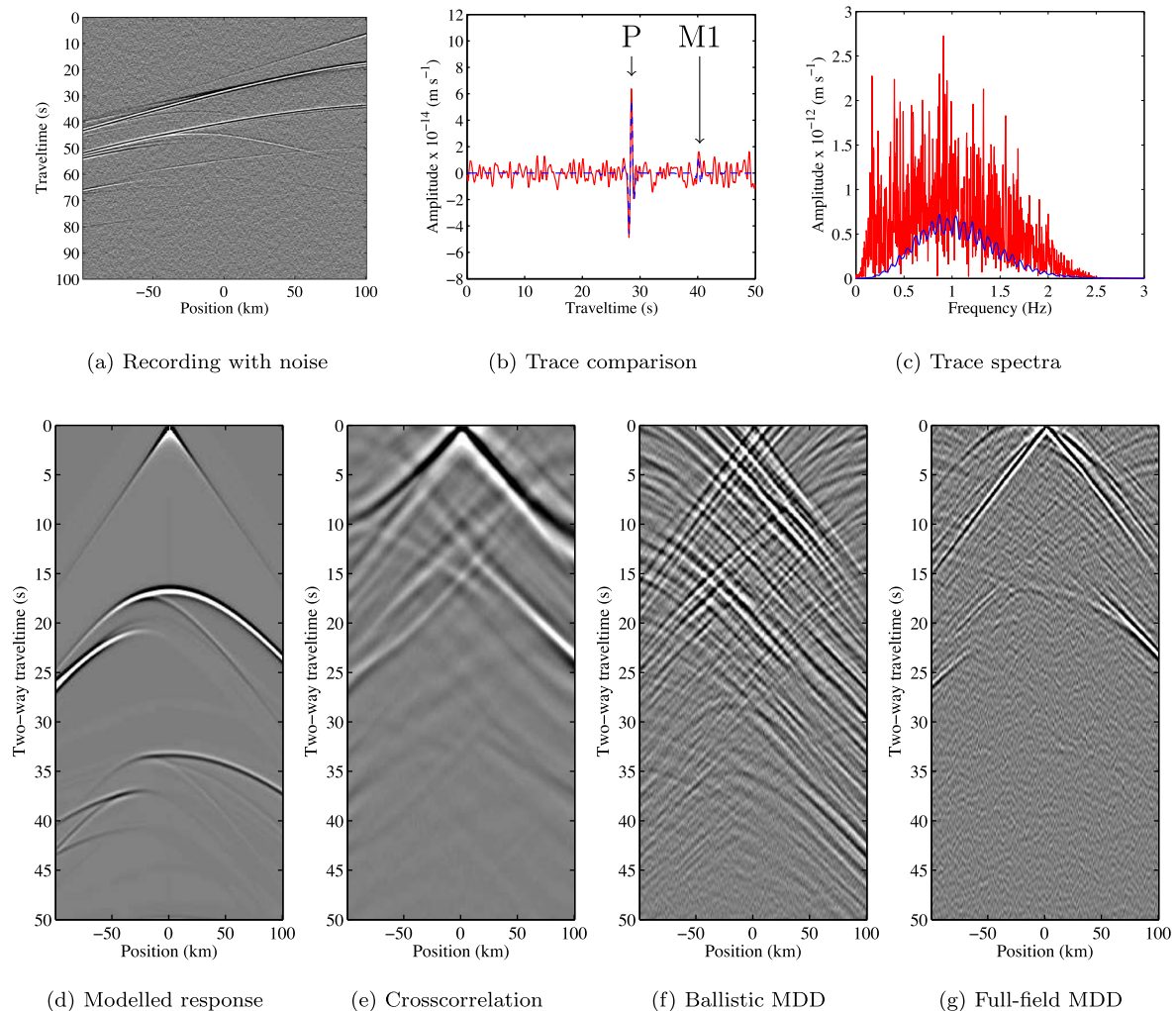
4 DISCUSSION

Earthquakes are generated by various complex mechanisms and are often sparsely distributed (Stein & Wysession 2003). Our re-

sults show that the quality of the body-wave reflections obtained by crosscorrelation and ballistic MDD is severely affected when these realistic conditions are met (Figs 4c and d). In contrast, full-field MDD turns out to be significantly less sensitive to the possible adverse effects of these circumstances and yields a complete retrieval of the body-wave reflection (Fig. 4e). Moreover, the addition of noise to the passive recordings does not significantly diminish the quality of the response retrieved by full-field MDD (Fig. 7g).

The robustness of full-field MDD can be explained by the fact that its kernel equals the full passive recording (eq. 7). As a consequence, its PSF takes into account additional wavenumber illumination provided by the scattered events contained in the recording and thus also corrects for the irregular illumination these events may cause. Another benefit of this kernel is that it does not require any approximations, which results in a more constrained and stable inversion.

Wavefields with high-frequency content are more sensitive to the various scales of heterogeneities present in a realistic lithospheric medium: the scattering potential will effectively increase with higher frequency content (Sato *et al.* 2012). A medium with a stronger scattering potential has the advantage of increasing the range of wavenumbers contained in the illuminating field, which full-field MDD profits from. However, when the scattered field energy increases with respect to the ballistic field energy, the direct-wave approximation in the correlation function of full-field MDD will become less reliable. This can lead to an increase in the error in the estimate of the reflection response. This expected trade-off requires further research. Crosscorrelation does not rely on the direct-wave approximation and, in theory, would also profit from a stronger scattering potential in case this generates isotropically scattered waves at the receiver level (Snieder 2004). However, a modelling study of coda-wave crosscorrelation interferometry showed that in case of only a slightly higher scattering potential, the reflection retrieval becomes obscured by the associated emergence of cross-talk artefacts (Hartstra & Wapenaar 2015).

Another characteristic of strongly scattering media is that *P*-to *S*-wave conversions dominate the multiply scattered wavefield

(a) Recording with noise   (b) Trace comparison   (c) Trace spectra

(d) Modelled response   (e) Crosscorrelation   (f) Ballistic MDD   (g) Full-field MDD

Figure 7. Limited high-angle illumination scenario as described in Fig. 4(a), but with added noise. (a) Vertical particle-velocity recording of a passive source with added noise (the clipping is slightly increased). (b) Trace at position 0 km of a passive recording with (red) and without noise (dashed blue). The arrow with 'P' indicates the Moho primary and 'M1' the first order free-surface multiple. (c) Spectrum of the trace in (b) with (red) and without noise (blue). (d) Modelled vertical particle-velocity reflection response to a vertical dipole-source placed at the middle receiver. (e) Vertical particle-velocity reflection response from passive recordings with noise using crosscorrelation. (f) Idem, using ballistic MDD. (g) Idem, using full-field MDD.

(Snieder 2002). We derived the full-field MDD equation for elasto-dynamic wavefields (eq. A14), which only requires particle-velocity recordings as input and possibly does not require surface-wave removal. Using full-field MDD, we expect to retrieve an elastodynamic reflection response of a comparable quality as for the acoustic case demonstrated here.

Finally, we would like to point out that this method is not limited to lithospheric imaging applications. Depending on the characteristics of the array, full-field MDD could be used to obtain body-wave reflections on a global scale to shed light on mantle and core structures (Ruigrok 2012). Additionally, the method could prove useful for monitoring purposes in marine ocean-bottom cable configurations by allowing the use of natural microseismic sources instead of active marine sources (Ravasi *et al.* 2015).

5 CONCLUSIONS

We derived a novel interferometric method by MDD for passive particle-velocity recordings at the free surface. The input data do not require wavefield decomposition and the retrieved reflection

response does not contain free-surface multiples. In the retrieval process, the additional wavenumbers provided by the passive coda wavefield are effectively used to cover illumination gaps. Moreover, the method intrinsically corrects for any illumination irregularities caused by both the passive sources and the scattering inside the medium. The numerical experiments showed that the inversion does not become unstable in the case of having noise-contaminated recordings of sparsely distributed passive sources with strongly varying radiation patterns. When compared to conventional passive SI approaches, this novel MDD method provides a more accurate result under these circumstances.

The Netherlands Research Centre for Integrated Solid Earth Science (ISES).

REFERENCES

Almagro Vidal, C., 2017. Passive seismic interferometry for reflection imaging and monitoring, *PhD thesis*, Delft University of Technology.

Arfken, G.B. & Weber, H.J., 2005. *Mathematical Methods for Physicists,* pp. 1023–1024, Academic Press.

Berkhout, A., 1982. *Seismic Migration: Imaging of Acoustic Energy by Wave Field Extrapolation,* Elsevier.

Boué, P., Poli, P., Campillo, M. & Roux, P., 2014. Reverberations, coda waves and ambient noise: correlations at the global scale and retrieval of the deep phases, *Earth planet. Sci. Lett.,* **391,** 137–145.

de Hoop, A.T., 1995. *Handbook of Radiation and Scattering of Waves,* 1st edn, Academic Press.

Draganov, D., Wapenaar, C.P.A., Mulder, W., Singer, J. & Verdel, A., 2007. Retrieval of reflections from seismic background-noise measurements, *Geophys. Res. Lett.,* **34,** L04305, doi:10.1029/2006GL028735.

Dziewonski, A.M. & Anderson, D.L., 1981. Preliminary reference earth model, *Phys. Earth planet. Inter.,* **25**(4), 297–356.

Fokkema, J.T. & van den Berg, P., 1993. *Seismic Applications of Acoustic Reciprocity,* Elsevier.

Hartstra, I. & Wapenaar, K., 2015. A method to retrieve an improved high resolution reflection response from HiCLIMB array recordings of local earthquake scattering coda, in *26th IUGG General Assembly,* Prague.

Nakata, N., Snieder, R. & Behm, M., 2014. Body-wave interferometry using regional earthquakes with multidimensional deconvolution after wavefield decomposition at free surface, *Geophys. J. Int.,* **199**(2), 1125–1137.

Nolet, G., 2008. *A Breviary of Seismic Tomography: Imaging the Interior of the Earth and Sun,* Cambridge Univ. Press.

Poli, P., Pedersen, H.A. & Campillo, M., 2012. Emergence of body waves from cross-correlation of short period seismic noise, *Geophys. J. Int.,* **188**(2), 549–558.

Ravasi, M., Meles, G., Curtis, A., Rawlinson, Z. & Yikuo, L., 2015. Seismic interferometry by multidimensional deconvolution without wavefield separation, *Geophys. J. Int.,* **202**(1), 1–16.

Ruigrok, E., 2012. Body-wave seismic interferometry applied to earthquake- and storm-induced wavefields, *PhD thesis*, Delft University of Technology.

Sato, H., Fehler, M.C. & Maeda, T., 2012. *Seismic Wave Propagation and Scattering in the Heterogeneous Earth,* 2nd edn, Springer.

Schuster, G.T., 2009. *Seismic Interferometry,* 1st edn, Cambridge Univ. Press.

Snieder, R., 2002. Coda wave interferometry and the equilibration of energy in elastic media, *Phys. Rev. E,* **66**(4), 046615, doi:10.1103/PhysRevE.66.046615.

Snieder, R., 2004. Extracting the Green's function from the correlation of coda waves: a derivation based on stationary phase, *Phys. Rev. E,* **69**(4), 046610, doi:10.1103/PhysRevE.69.046610.

Stein, S. & Wysession, M., 2003. *An Introduction to Seismology, Earthquakes, and Earth Structure,* Blackwell Publishing.

Thorbecke, J.W. & Draganov, D., 2011. Finite-difference modeling experiments for seismic interferometry, *Geophysics,* **76,** H1–H18.

Tonegawa, T., Nishida, K., Watanabe, T. & Shiomi, K., 2009. Seismic interferometry of teleseismic *S*-wave coda for retrieval of body waves: an application to the Philippine sea slab underneath the Japanese Islands, *Geophys. J. Int.,* **178,** 1574–1586.

van der Neut, J., 2012. Interferometric redatuming by multidimensional deconvolution, *PhD thesis*, Delft University of Technology.

van der Neut, J. & Herrmann, F.J., 2013. Interferometric redatuming by sparse inversion, *Geophys. J. Int.,* **192,** 666–670.

van der Neut, J., Tatanova, M., Thorbecke, J., Slob, E. & Wapenaar, K., 2011. Deghosting, demultiple, and deblurring in controlled-source seismic interferometry, *Int. J. Geophys.,* **2011,** 870819, doi:10.1155/2011/870819.

Wapenaar, K., 1996. One-way representations of seismic data, *Geophysic. J. Int.,* **127,** 178–188.

Wapenaar, K. & Fokkema, J., 2006. Green's function representations for seismic interferometry, *Geophysics,* **71,** SI33–SI46.

Wapenaar, K., van der Neut, J. & Ruigrok, E., 2008. Passive seismic interferometry by multidimensional deconvolution, *Geophysics,* **73**(6), A51–A56.

Wapenaar, K., van der Neut, J., Ruigrok, E., Draganov, D., Hunziker, J., Slob, E., Thorbecke, J. & Snieder, R., 2011. Seismic interferometry by crosscorrelation and by multidimensional deconvolution: a systematic comparison, *Geophys. J. Int.,* **185,** 1335–1364.

APPENDIX A: DERIVATION OF FULL-FIELD MDD

Following Wapenaar & Fokkema (2006), we derive the full-field MDD relation for elastodynamic wavefields in an arbitrary inhomogeneous isotropic domain $\mathbb{D}$ with boundary $\partial\mathbb{D}$ and outward pointing normal vector n_j (see Fig. 2). We define two independent states A and B in the same domain $\mathbb{D}$ and introduce the local interaction quantity $\partial_j \left[\hat{v}_i^A \hat{\tau}_{ij}^B - \hat{\tau}_{ij}^A \hat{v}_i^B \right]$ to relate fields in the respective states (Fokkema & van den Berg 1993; de Hoop 1995; Wapenaar 1996), where 'hat' indicates the space-frequency domain. Capital superscripts denote which state the field belongs to, while lower-case subscripts indicate the component of each field, which can take up values 1, 2 and 3. The number of subscript letters designates the order of the tensor. Note that Einstein's summation convention holds here. The particle velocity is denoted by $\hat{v}_i$ and the tensorial stress field by $\hat{\tau}_{ij}$, where $i = j$ denotes normal stress and $i \neq j$ shear stress. We substitute Newton's second law and Hooke's law into the local interaction quantity and apply Gauss' theorem, yielding global reciprocity theorem:

$$\oint_{\partial\mathbb{D}} \left[\hat{v}_i^A \hat{\tau}_{ij}^B - \hat{\tau}_{ij}^A \hat{v}_i^B \right] n_j \mathrm{d}^2\mathbf{x}$$
$$= \int_{\mathbb{D}} \left[-\hat{\tau}_{ij}^A \hat{h}_{ij}^B - \hat{v}_i^A \hat{f}_i^B + \hat{h}_{ij}^A \hat{\tau}_{ij}^B + \hat{f}_i^A \hat{v}_i^B \right] \mathrm{d}^3\mathbf{x}, \qquad (A1)$$

where $\hat{f}_i$ denotes the force density source and $\hat{h}_{ij}$ is the uniaxial shear density for $i = j$ and simple shear density source for $i \neq j$. In the following we assume that the medium parameters in $\mathbb{D}$ are the same in both states. In both states A and B, we divide the boundary of domain $\mathbb{D}$ into a horizontal acquisition surface defined by the receiver positions, $\mathbf{x}_R \in \partial\mathbb{D}_R$, and a half-sphere in the subsurface, $\partial\mathbb{D}_M$, which has absorbing boundary conditions in both states A and B. The boundary condition at $\partial\mathbb{D}_R$ differs between the two states: in state A it has absorbing boundary conditions, while in state B, it forms a free surface. The opposite is the case for the derivation of ballistic MDD by Wapenaar *et al.* (2008; Fig. 1). The sources in state A are located at $\mathbf{x}_A$ just inside the domain immediately below the boundary $\partial\mathbb{D}_R$. In state B, the source locations $\mathbf{x}_B$ are located at arbitrary positions inside the domain $\mathbb{D}$. Since the final solution is independent of passive-source type, we take the liberty to neglect the $\hat{h}_{ij}$ sources. By extending boundary $\partial\mathbb{D}_M$ to infinity, the contribution of that part of the integral vanishes due to Sommerfeld's radiation condition. This results in

$$\int_{\partial\mathbb{D}_R} \left[\hat{v}_i^o \hat{\tau}_{ij} - \hat{\tau}_{ij}^o \hat{v}_i \right] n_j \mathrm{d}^2\mathbf{x} = \int_{\mathbb{D}} \left[-\hat{v}_i^o \hat{f}_i + \hat{f}_i^o \hat{v}_i \right] \mathrm{d}^3\mathbf{x}, \qquad (A2)$$

where we also simplified the notation by denoting all wavefields of state A, which are without free-surface interaction, with a superscript 'o', while wavefields in state B, which do have free-surface interaction, have no superscript. The field $\hat{\tau}_{ij} n_j$ does not contribute

to the integral, because the acquisition surface $\partial \mathbb{D}_R$ coincides with the free surface of state B. Of the remaining field in the integrand, only the components perpendicular to the horizontal boundary $\partial \mathbb{D}_R$, which has an upward pointing normal vector, contribute to the integral: $\hat{\tau}^o_{ij} n_j \rightarrow -\hat{\tau}^o_{i3}$. Applying these constraints imposed by the boundary yields:

$$\int_{\partial \mathbb{D}_R} \hat{\tau}^o_{i3} \hat{v}_i \mathrm{d}^2 \mathbf{x}_R = \int_{\mathbb{D}} \left[\hat{f}^o_i \hat{v}_i - \hat{v}^o_i \hat{f}_i \right] \mathrm{d}^3 \mathbf{x}. \tag{A3}$$

We now proceed to define the source terms as impulsive functions and consequently the wavefield terms as Green's functions:

$$\hat{f}^o_i = \delta(\mathbf{x} - \mathbf{x}_A)\delta_{ik}, \tag{A4}$$

$$\hat{v}^o_i = \hat{G}^o_{i|k}(\mathbf{x}, \mathbf{x}_A, \omega), \tag{A5}$$

$$\hat{\tau}^o_{i3} = \hat{G}^o_{i3|k}(\mathbf{x}, \mathbf{x}_A, \omega), \tag{A6}$$

$$\hat{f}_i = \delta(\mathbf{x} - \mathbf{x}_B)\delta_{iq}, \tag{A7}$$

$$\hat{v}_i = \hat{G}_{i|q}(\mathbf{x}, \mathbf{x}_B, \omega), \tag{A8}$$

where ω denotes the angular frequency. The lower-case subscripts, with possible values 1, 2 or 3, on the left-hand side of the vertical bar denote the receiver component of the field, while subscripts on the right-hand side denote the component of the source mechanism. Substituting these expressions in the global reciprocity theorem (A3), we solve the domain integral and apply the source-receiver reciprocity relations $\hat{G}^o_{k|i3}(\mathbf{x}_A, \mathbf{x}, \omega) = \hat{G}^o_{i3|k}(\mathbf{x}, \mathbf{x}_A, \omega)$ and $\hat{G}^o_{k|i}(\mathbf{x}_A, \mathbf{x}, \omega) = \hat{G}^o_{i|k}(\mathbf{x}, \mathbf{x}_A, \omega)$. The final result becomes

$$\int_{\partial \mathbb{D}_R} \hat{G}^o_{k|i3}(\mathbf{x}_A, \mathbf{x}_R, \omega)\hat{G}_{i|q}(\mathbf{x}_R, \mathbf{x}_B, \omega)\mathrm{d}^2 \mathbf{x}_R$$

$$= \hat{G}_{k|q}(\mathbf{x}_A, \mathbf{x}_B, \omega) - \hat{G}^o_{k|q}(\mathbf{x}_A, \mathbf{x}_B, \omega), \tag{A9}$$

where $\hat{G}^o_{k|i3}(\mathbf{x}_A, \mathbf{x}_R, \omega)$ is the particle-velocity response at $\mathbf{x}_A$ to an impulsive shear density source at $\mathbf{x}_R$. Since $\mathbf{x}_A$ and $\mathbf{x}_R$ are immediately below and at the surface, respectively, $\hat{G}^o_{k|i3}(\mathbf{x}_A, \mathbf{x}_R, \omega)$ represents an impulsive reflection response (including the direct wave). Hence, we change its notation to

$$\hat{R}^o_{k|i3}(\mathbf{x}_A, \mathbf{x}_R, \omega) = \hat{G}^o_{k|i3}(\mathbf{x}_A, \mathbf{x}_R, \omega). \tag{A10}$$

We denote the particle-velocity field measured at the free surface due to an impulsive force at $\mathbf{x}_B$ with source spectrum $\hat{S}(\omega)$ as

$$\hat{V}_{i|q}(\mathbf{x}_R, \mathbf{x}_B, \omega) = \hat{G}_{i|q}(\mathbf{x}_R, \mathbf{x}_B, \omega)\hat{S}(\omega). \tag{A11}$$

The full response of the medium without free surface is presented as

$$\hat{V}^o_{k|q}(\mathbf{x}_A, \mathbf{x}_B, \omega) = \hat{G}^o_{k|q}(\mathbf{x}_A, \mathbf{x}_B, \omega)\hat{S}(\omega), \tag{A12}$$

and the full response of the medium with free surface is

$$\hat{V}_{k|q}(\mathbf{x}_A, \mathbf{x}_B, \omega) = \hat{G}_{k|q}(\mathbf{x}_A, \mathbf{x}_B, \omega)\hat{S}(\omega). \tag{A13}$$

Substituting definitions (A10)–(A13) into eq. (A9) yields the final elastodynamic full-field MDD relation

$$\int_{\partial \mathbb{D}_R} \hat{R}^o_{k|i3}(\mathbf{x}_A, \mathbf{x}_R, \omega)\hat{V}_i(\mathbf{x}_R, \mathbf{x}_B, \omega)\mathrm{d}^2 \mathbf{x}_R$$

$$= \hat{V}_k(\mathbf{x}_A, \mathbf{x}_B, \omega) - \hat{V}^o_k(\mathbf{x}_A, \mathbf{x}_B, \omega), \tag{A14}$$

where we omitted subscript 'q', because the passive-source mechanism does not influence the left-hand side of the equation. The desired $\hat{R}^o_{k|i3}(\mathbf{x}_A, \mathbf{x}_R, \omega)$ is the particle-velocity reflection response of the medium without free surface at $\mathbf{x}_A$ due to a uniaxial or simple shear source, depending on subscript 'i', at position $\mathbf{x}_R$ at the horizontal surface. Note that the surface orientation defines the virtual source orientation of the reflection response retrieval. The acoustic form of the equation is

$$\int_{\partial \mathbb{D}_R} \hat{R}^o_{k|0}(\mathbf{x}_A, \mathbf{x}_R, \omega)\hat{V}_3(\mathbf{x}_R, \mathbf{x}_B, \omega)\mathrm{d}^2 \mathbf{x}_R$$

$$= \hat{V}_k(\mathbf{x}_A, \mathbf{x}_B, \omega) - \hat{V}^o_k(\mathbf{x}_A, \mathbf{x}_B, \omega), \tag{A15}$$

whereby $\hat{R}^o_{k|0}(\mathbf{x}_A, \mathbf{x}_R, \omega)$ is the particle-velocity reflection response at $\mathbf{x}_A$ due to a scalar monopole source, indicated by source subscript zero '0', at $\mathbf{x}_R$. Note that $\hat{V}^o_k(\mathbf{x}_A, \mathbf{x}_B, \omega)$ can only be obtained by removing the free-surface multiples from the passive recorded field $\hat{V}_k(\mathbf{x}_A, \mathbf{x}_B, \omega)$. Since this is difficult to achieve in practice, the field can instead be approximated by selecting the direct wave of the passive recording and multiplying it by $\frac{1}{2}$ to remove the effect of the free surface. However, in the case of elastodynamic full-field MDD (eq. A14) this approximation does not suffice. Instead, wave-field decomposition is required to remove the effect of the free surface from the direct P and S waves.